Structural and Electron-Transfer Characteristics of Carbon-Tethered Porphyrin Monolayers on Si(100)

Lingyun Wei,[†] Dennis Syomin,[†] Robert S. Loewe,[‡] Jonathan S. Lindsey,*[,‡] Francisco Zaera,*[,†] and David F. Bocian*[,†]

Departments of Chemistry, University of California, Riverside, California 92521-0403, and North Carolina State University, Raleigh, North Carolina 27695-8204

Received: November 30, 2004; In Final Form: January 28, 2005

Structural and electron-transfer characteristics are reported for two classes of zinc porphyrin monolayers attached to Si(100) surfaces via Si−C bonds. One class, designated ZnP$(CH_2)_n$− (n = 2−4), contains an alkyl linker appended to the *meso*-position of the porphyrin, with the nonlinking substituents being *p*-tolyl groups. The other, designated ZnPPh$(CH_2)_n$− (n = 0−3), contains a phenyl or phenylalkyl linker appended to the *meso*-position of the porphyrin, with the nonlinking substituents being mesityl groups. Both classes of zinc porphyrin monolayers on Si(100) were examined using Fourier transform infrared spectroscopy and various electrochemical methods. The studies reveal the following: (1) The structural and electron-transfer characteristics of the ZnP$(CH_2)_n$− and ZnPPh$(CH_2)_n$− monolayers are generally similar to those of monolayers formed from porphyrins with analogous linkers, but anchored with an O, a S, or a Se atom. (2) The ZnP$(CH_2)_n$−, ZnPPh−, and ZnPPhCH_2− monolayers exhibit lower saturation coverages and have their porphyrin ring more tilted with respect to the surface normal than the ZnPPh$(CH_2)_2$− and ZnPPh$(CH_2)_3$− monolayers. (3) The electron-transfer rates for both the ZnP$(CH_2)_n$− and ZnPPh$(CH_2)_n$− classes of monolayers monotonically decrease as the length of the linker increases. (4) For all the ZnP$(CH_2)_n$− and ZnPPh$(CH_2)_n$− monolayers, both electron-transfer rates and charge-dissipation rates decrease monotonically as the surface coverage increases. Collectively, the studies reported herein provide a detailed picture of how the linker type influences the structural and electron-transfer characteristics of these general classes of monolayers.

I. Introduction

The prospect that devices relying on the bulk properties of semiconductors will fail to retain their characteristic properties as their sizes reach nanoscale dimensions has motivated a desire to implement molecular materials as the active media in electronic devices.[1] The step to molecular-based devices will likely proceed through transition technologies wherein molecular materials are first integrated with semiconductors, thereby capitalizing on the vast infrastructure of the semiconductor industry. Toward this goal, we have been engaged in a program aimed at constructing devices that use the properties of molecules to store information.[2,3] In this approach a collection of redox-active molecules attached to an electroactive surface serves as the active storage medium, and information is stored in the discrete redox states of the molecules.

Our hybrid molecular/semiconductor architectures have principally used porphyrins as the electroactive medium and Si(100) as the semiconductor platform.[3] A key structural feature of the porphyrin−Si hybrid is the nature of the anchor atom between the molecule and the surface. Our initial designs using O atom anchors[3a,b] have been extended recently to include both S and Se atom tethers.[3c] The Si−O, Si−S, and Si−Se covalent linkages were formed via a thermal procedure[4] that exploits the excellent stability of porphyrins at high temperatures (400 °C and greater).[3b] In the course of this work, we further demonstrated that the thermal procedure affords facile attachment of porphyrins to Si(100) via a C atom anchor.[4] The Si−C linkages can be formed from a variety of functional groups, including alkyl and aryl halides, alkenes, and alkynes. While there are numerous reports describing attachment of organic molecules to Si surfaces, including via Si−C bonds,[5] limited data are available for electroactive monolayers tethered via Si−C linkages.[4,6] The availability of porphyrin monolayers anchored to Si via a C atom permits comparison of the physical characteristics of this architecture with those of porphyrin monolayers anchored by group VI atoms. Ultimately, a hybrid porphyrin−Si architecture based on Si−C linkages may prove more attractive for device applications than those based on a Si−group VI atom linkage because the Si−C bond is not susceptible to hydrolysis.

Herein, we examine the structural and electron-transfer characteristics of two classes of zinc porphyrin monolayers attached to Si(100) surfaces via Si−C bonds. One class of molecules, designated ZnP$(CH_2)_n$− (n = 2−4), contains an alkyl linker appended to the *meso*-position of the porphyrin, with the nonlinking substituents being *p*-tolyl groups. The other class, designated ZnPPh$(CH_2)_n$− (n = 0−3), contains a phenyl or phenylalkyl linker appended to the *meso*-position of the porphyrin, with the nonlinking substituents being mesityl groups. The structures of ZnP$(CH_2)_n$− and ZnPPh$(CH_2)_n$− are shown in Chart 1, along with those of the ZnPX (**1**−**3**) and ZnPPhX (**4**−**7**) molecules that were used to prepare the monolayers. Both classes of zinc porphyrin monolayers on Si(100) were examined

* To whom correspondence should be addressed. E-mail: jlindsey@ncsu.edu (J.S.L.); Francisco.Zaera@ucr.edu (F.Z.); David.Bocian@ucr.edu (D.F.B.).

[†] University of California.

[‡] North Carolina State University.

10.1021/jp044558v CCC: $30.25
Published on Web 03/05/2005

CHART 1: Structures of the Surface-Attached $ZnP(CH_2)_n-$ and $ZnPPh(CH_2)_n-$ Porphyrins and the ZnPX (1−3) and ZnPPhX (4−7) Porphyrins Used for Preparing the Monolayers

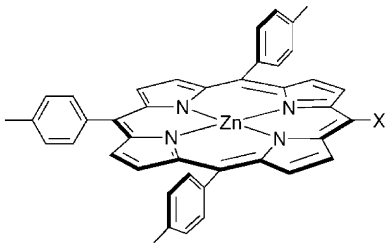

Compound: X	Surface-attached species
1: -CH=CH_2	**$ZnP(CH_2)_2$-**
2: -CH_2CH=CH_2	**$ZnP(CH_2)_3$-**
3: -CH_2CH_2CH=CH_2	**$ZnP(CH_2)_4$-**

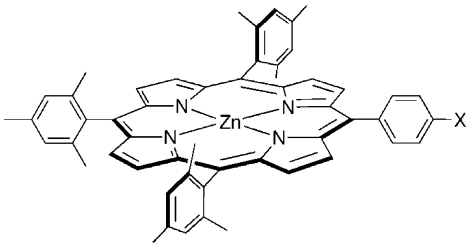

Compound: X	Surface-attached species
4: -I	**ZnPPh-**
5: -CH_2Br	**$ZnPPhCH_2$-**
6: -CH=CH_2	**$ZnPPh(CH_2)_2$-**
7: -CH_2CH=CH_2	**$ZnPPh(CH_2)_3$-**

using Fourier transform infrared (FTIR) spectroscopy to measure the relative orientations of the porphyrin rings with respect to the surface plane, fast-scan cyclic voltammetry to quantitate the packing densities of the monolayers, swept waveform ac voltammetry (SWAV) to elucidate the kinetics of electron transfer,[2d] and open circuit potential amperometry (OCPA) to determine the time of charge retention after the removal of applied potential.[2c]

II. Experimental Section

A. Chemicals and Materials. ZnPX (**1**−**3**) and ZnPPhX (**4**−**7**) were synthesized as described previously.[4] The solvents used in the preparation of the monolayers and the electrochemical measurements were anhydrous CH_2Cl_2 (Aldrich, 99%), anhydrous benzonitrile (Aldrich, 99%), and propylene carbonate (Aldrich, 99%). The *n*-Bu_4NPF_6 (Aldrich) supporting electrolyte was recrystallized three times from methanol and dried in a vacuum at 110 °C.

Silicon (100) wafers (Silicon Valley Microelectronics) were purchased as thermally oxidized B-doped (p-type) Si(100) (ρ = 0.01−0.03 Ω·cm) and nonoxidized B-doped Si(100) (ρ = 10−30 Ω·cm). The low- and high-resistivity materials were used for the electrochemical and FTIR experiments, respectively; high-resistivity Si(100) is required for the FTIR experiments to minimize infrared absorption by the charge carriers in the bulk. The chemicals used in Si microelectrode fabrication were AZ 5214 positive photoresist (Baker), AZ 400K photoresist developer (Baker), Baker Aleg 355 resist stripper (Baker), nanostrip (Cyantek), HF dip (5:1), buffered oxide etch, and J. T. Baker clean (Baker). Ar and N_2 (99.995%) were passed through Drierite (Fisher) and Oxyclear (Supelco) gas purifiers prior to use. Deionized water (from a Milli-Q system) had a ρ > 16 MΩ·cm.

B. Electrode Preparation. The electrochemical measurements on the monolayers were made using highly doped p-type Si(100) working microelectrodes (100 × 100 μm) prepared via photolithographic methods as described previously.[3a] A microelectrode was used to ensure that the RC time constant of the electrochemical cell was sufficiently short so that the electron-transfer kinetics of the porphyrin monolayers could be measured accurately.

A bare Ag wire was used as the counter/reference electrode. The electrode was prepared by sonicating a section of 500 μm diameter Ag wire (Alfa Aesar) in 7.0 M NH_4OH, rinsing it in deionized water and ethanol, and then sonicating it in CH_2Cl_2 containing 1.0 M *n*-Bu_4NPF_6. The Ag wire prepared in this manner was placed inside a 10 μL polypropylene pipet tip containing ∼5 μL of the propylene carbonate/1.0 M *n*-Bu_4NPF_6 electrolyte solution and manipulated using a micropositioning device in a setup previously described.[3a]

C. Monolayer Preparation. All of the monolayers were assembled on hydrogen-passivated Si(100) surfaces, prepared as described previously,[3a] by using a high-temperature (400 °C), short-time (2 min) "baking" attachment procedure previously shown to give facile attachment of porphyrins **1**−**7** to Si(100) surfaces.[4] The surface coverage and conditions for achieving saturation coverage were determined electrochemically in a series of experiments wherein the concentration of the porphyrin in the deposition solution (benzonitrile) was varied systematically. These experiments revealed that the surface coverage could be varied in a controlled fashion in the low 10^{-12} to the mid 10^{-11} mol cm^{-2} range (saturation coverage) by varying the porphyrin concentration from ∼2 μM to ∼2 mM.

The monolayers for the electrochemical experiments were prepared by dispensing a 2 μL drop of the porphyrin solution onto the surface of the microelectrode contained in a sparged VOC vial sealed under Ar. The monolayers prepared for the FTIR experiments utilized much larger platforms (∼1 cm^2), and consequently required a larger drop size, ∼50 μL. After deposition, the vial containing the Si substrate was heated on a hot plate at 400 °C for 2 min, then removed, and purged with Ar until it cooled to room temperature. Finally, the Si substrate was rinsed and sonicated five times with anhydrous CH_2Cl_2 and purged dry once again under Ar.

D. FTIR Spectroscopy. The FTIR spectra of the porphyrins in both solid and monolayer forms were collected at room temperature using a Bruker Tensor 27 FTIR spectrometer. In all cases, a spectral resolution of 4 cm^{-1} was used.

The spectra of solid ZnPX (**1**−**3**) and ZnPPhX (**4**−**7**) (Chart 1) were obtained in KBr pellets (∼1−2 wt % porphyrin). These spectra were collected in transmission mode using a room temperature DTGS detector by averaging over 32 scans.

The IR spectra of the Si−H_x surface and the $ZnP(CH_2)_n-$ and $ZnPPh(CH_2)_n-$ monolayers were obtained using a Harrick Scientific horizontal reflection Ge attenuated total reflection accessory (GATR; 65° incidence angle). The Si substrates were placed in contact with the flat surface of a semispherical Ge crystal that serves as the optical element, and IR spectra were collected with p-polarized light using a liquid-nitrogen-cooled medium-bandwidth (600−4000 cm^{-1}) MCT detector and averaging over 256 scans. The IR spectra of the Si−H_x surface were obtained as the ratio of the single beam spectrum of the HF-etched Si(100) surface against that of a Si(100) sample with a native oxide film. The spectra of the porphyrin monolayers

were referenced against that of a hydrogen-terminated Si(100) surface previously subjected to the same deposition conditions as those used to obtain the monolayer but using only the neat deposition solvent. The Ge crystal was cleaned with neat 2-butanone before every experiment, and the GATR accessory was purged with dry N_2 during data acquisition.

E. Electrochemical Measurements. The electrochemical measurements on the porphyrins in solution were made in a standard three-electrode cell using Pt working and counter electrodes and a Ag/Ag^+ reference electrode. The solvent/electrolyte was CH_2Cl_2 containing 1.0 M Bu_4NPF_6. The electrochemical measurements on the monolayers were performed in a two-electrode configuration using the fabricated Si(100) microelectrode and the Ag counter/reference electrode described earlier,[3a] and propylene carbonate containing 1.0 M Bu_4NPF_6 as the solvent/electrolyte. The RC time constant for this microelectrode/electrochemical cell, measured to be $\sim 4\ \mu s$, is sufficiently short to preclude any significant interference with the measurement of the electron-transfer rates. The cyclic voltammograms were recorded using a Gamry Instruments PC4-FAS1 femtostat running PHE 200 Framework and Echem Analyst software. The surface coverage of the porphyrins in the monolayer was determined by integration of the total charge in the first anodic wave and by using the geometric dimensions of the microelectrode. The standard electron-transfer rate constants, k^0, of the porphyrin monolayers were obtained using the same SWAV method previously used to obtain k^0 values for porphyrin monolayers on both Au and Si surfaces.[2a,c−g] The rates of charge dissipation after disconnection from the applied potential, reported as charge-retention half-lives, $t_{1/2}$, were obtained using the OCPA method also used previously to obtain $t_{1/2}$ values for porphyrin monolayers on both Au and Si surfaces.[2,3a]

III. Results

A. FTIR Studies. A series of FTIR studies were conducted to investigate the structure of the porphyrins and their adsorption geometry in the monolayers. The midfrequency (700−1900 cm^{-1}) IR spectra of the saturation-coverage $ZnP(CH_2)_n-$ and $ZnPPh(CH_2)_n-$ monolayers are shown as the bottom trace of each pair of traces in Figures1 and 2, respectively, and those of solid samples of the parent ZnPX (**1**−**3**) and ZnPPhX (**4**−**7**) porphyrins are shown as the top trace of each pair of traces for comparison. The spectra of the monolayers are plotted on the same absolute intensity scale to allow for the comparison of the relative intensities of the bands. All of the spectra exhibit numerous bands in this frequency region, which previous studies of structurally related porphyrins have shown to be due mostly to in-plane modes of the porphyrin ring or the aryl substituents. Two features in these spectra are of particular relevance to our studies, the porphyrin pyrrole in-plane ring breathing mode near 998 cm^{-1},[7] and the out-of-plane β-pyrrole hydrogen deformation at 797 cm^{-1}.[8] For all of the original solid vinyl-functionalized porphyrins, ZnPX (**1**−**3**) and ZnPPhX (**6, 7**), additional bands are observed in the 1625−1640 cm^{-1} range associated with the C═C stretching vibration, ν(C═C), and in the 905−915 cm^{-1} range due to an out-of-plane C−H deformation, γ(CH).[9] Only weak bands are seen in the high-frequency (2600−3400 cm^{-1}) spectral region (not shown), all attributable to C−H stretches.

A number of key features are observed in the IR spectra of the monolayers, including the following.

(1) The spectra for the monolayer and solid samples of a given type of porphyrin are quite similar. This indicates that the structure of the porphyrin macrocycle and substituent groups is retained upon monolayer formation.

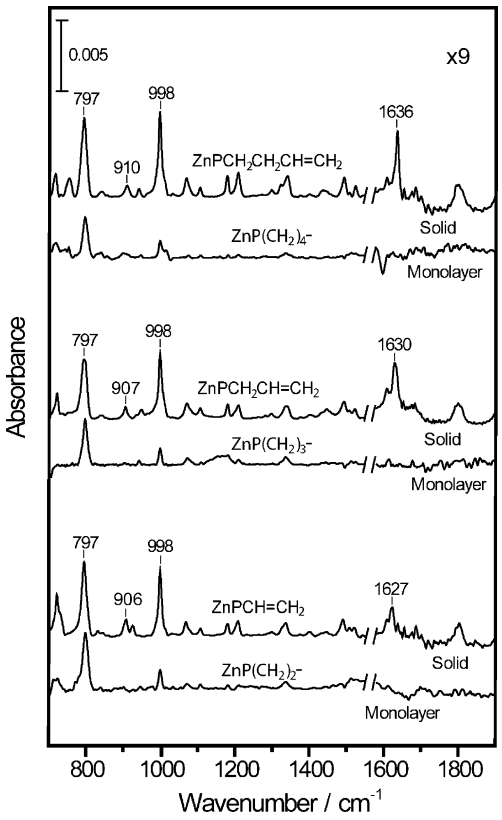

Figure 1. FTIR spectra of the solid ZnPX porphyrins (**1**−**3**) in KBr pellets and the corresponding $ZnP(CH_2)_n-$ monolayers on Si(100).

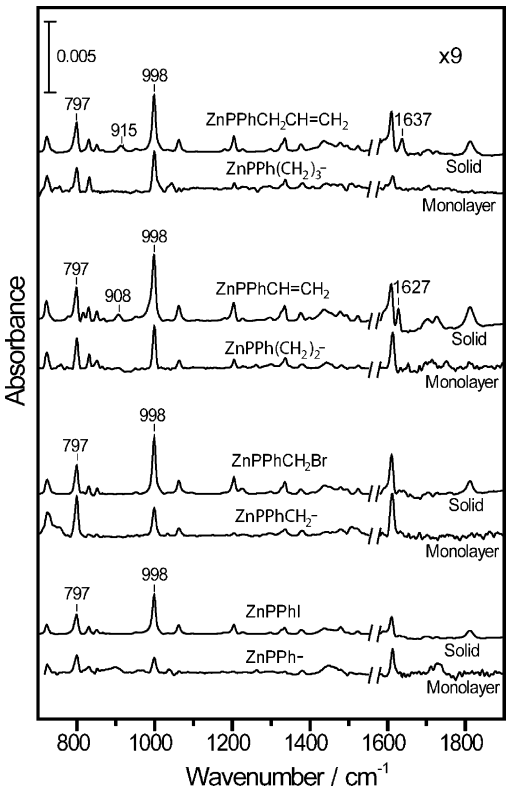

Figure 2. FTIR spectra of the solid ZnPPhX porphyrins (**4**−**7**) in KBr pellets and the corresponding $ZnPPh(CH_2)_n-$ monolayers on Si(100).

(2) The bands due to the ν(C═C) (1625−1640 cm^{-1}) and γ(CH) (905−915 cm^{-1}) vibrations are absent from the spectra of the monolayers formed from the vinyl-functionalized porphyrins, indicating saturation of the double bond in the alkene linker upon binding to the Si(100) surface, as expected for the

TABLE 1: Redox Potentials, Surface Coverage Values, and Average Tilt Angles for the ZnPPh$(CH_2)_n$- and ZnP$(CH_2)_n$- Monolayers on Si(100)

porphyrin		$E^{0/+1}$ (V)		$E^{+1/+2}$ (V)		$\Gamma \times 10^{-11}$ [c]	tilt, α [d]
soln	monolayer	soln[a]	monolayer[b]	soln[a]	monolayer[b]	(mol cm^{-2})	(deg)
1	ZnP$(CH_2)_2-$	0.53	0.58	0.81	0.92	5.2	50
2	ZnP$(CH_2)_3-$	0.53	0.55	0.85	0.91	5.9	49
3	ZnP$(CH_2)_4-$	0.51	0.54	0.86	0.91	6.2	48
4	ZnPPh$-$	0.56	0.59	0.91	0.96	6.2	47
5	ZnPPhCH_2-	0.56	0.64	0.90	1.00	7.3	50
6	ZnPPh$(CH_2)_2-$	0.54	0.62	0.90	0.98	8.3	40
7	ZnPPh$(CH_2)_3-$	0.54	0.62	0.92	0.98	9.7	37

[a] Solution potentials, obtained in CH_2Cl_2 containing 1.0 M *n*-Bu_4NPF_6; scan rate 0.1 V s^{-1}. Values are referenced vs Ag/Ag$^+$; $FeCp_2/FeCp_2^+$ 0.19 V. [b] Monolayer potentials, obtained in propylene carbonate containing 1.0 M *n*-Bu_4NPF_6; scan rate 100 V s^{-1}. [c] Porphyrin surface concentration, calculated from the integrated area of the $E^{0/+1}$ anodic wave, using the geometrical area of the microelectrode (1×10^{-4} cm^2). [d] Average tilt angle calculated on the basis of the intensity ratio of the out-of-plane β-pyrrole hydrogen deformation (797 cm^{-1}) and the in-plane pyrrole breathing (998 cm^{-1}) band in the infrared spectra.

hydrosilylation reaction that occurs when alkenes react with hydrogen-passivated Si.[5b,d]

(3) No clear bands are observed in the spectra of the monolayers that can be attributed to the stretching of the new Si$-$C bond, ν(Si$-$C), (expected in the 750$-$800-cm^{-1} range[5b,d]), most likely because of the low infrared absorption cross section and/or the low concentrations of those bonds on the surface. It is worth pointing out that although all of the Si$-$H$_x$ groups are eliminated from the surface during the surface-attachment reaction (as revealed by FTIR studies), less than 10% of the Si sites are occupied by the porphyrins (owing to the relatively large size of those molecules). The remainder of the Si sites are occupied by adventitious adducts, including solvent, residual water, or other organic materials present in small quantities, primarily anchored via Si$-$C and Si$-$O bonds (again as revealed by XPS and FTIR studies).

(4) The relative IR intensities of the in-plane (e.g., 998 cm^{-1}) versus out-of-plane (797 cm^{-1}) porphyrin modes are different for the monolayers versus the solids. These differences are the most apparent for the ZnP$(CH_2)_n-$ class of monolayers (Figure 1), and indicate a preferential ordered orientation of the adsorbed molecules with respect to the plane of the surface.

Regarding the latter point, the relative intensities of the in-plane versus out-of-plane porphyrin modes can be used to determine the average tilt angle (α) of the porphyrin ring with respect to the surface normal (Table 1).[10-14] The average angles determined from the IR data in Figure 1 for the ZnP$(CH_2)_n-$ monolayers are all quite similar to one another (ZnP$(CH_2)_2-$, $\alpha \approx 50°$; ZnP$(CH_2)_3-$, $\alpha \approx 49°$; ZnP$(CH_2)_4-$, $\alpha \approx 48°$) and similar to those we have previously observed for monolayers containing the structurally similar species ZnPCH_2X$-$ ($\alpha \approx 50°$) and ZnPPhCH_2X$-$ ($\alpha \approx 37°$), where X = O, S, and Se.[3c] The average tilt angles for the two shortest tethered members of the ZnPPh$(CH_2)_n-$ set, as estimated from the data in Figure 2, are also similar to one another (ZnPPh$-$, $\alpha \approx 49°$; ZnPPhCH_2-, $\alpha \approx 50°$) and similar to those of the ZnP$(CH_2)_n-$ series. On the other hand, the average tilt angles for the two longest tethered members of the ZnPPh$(CH_2)_n-$ set (ZnPPh$(CH_2)_2-$, $\alpha \approx 40°$; ZnPPh$(CH_2)_3-$, $\alpha \approx 37°$) are similar to one another but noticeably lower ($\sim$10°) that those of the other monolayers. We note that the fact that the ZnPX and ZnPPhX molecules contain different types of nonlinking substituents (*p*-tolyl versus mesityl; see Chart 1) is unlikely to play a significant role in determining the average tilt angle for the monolayers and explain the differences seen here between the two classes of monolayers. This assertion is based on our previous studies of structurally similar monolayers anchored to Si(100) via O, S, and Se atoms, which revealed that porphyrins with *p*-tolyl and mesityl nonlinking substituent groups exhibit similar average tilt angles.[3c]

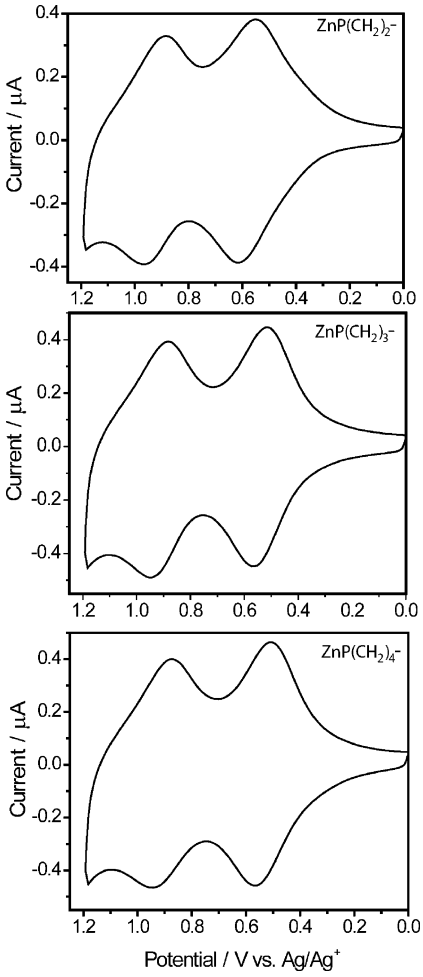

Figure 3. Representative fast-scan (100 V s^{-1}) voltammograms of the ZnP$(CH_2)_n-$ monolayers on Si(100).

B. Electrochemical Studies. *1. Voltammetric Characteristics.* Representative fast scan (100 V s^{-1}) cyclic voltammograms for the saturation-coverage ZnP$(CH_2)_n-$ and ZnPPh$(CH_2)_n-$ monolayers on Si(100) microelectrodes are shown in Figures 3 and 4, respectively. At oxidizing potentials, each monolayer exhibits two resolved voltammetric waves indicative of formation of the mono- and dication porphyrin π-radicals. The redox potentials for the different monolayers and the surface concentrations, Γ, at saturation coverage derived from these data are summarized in Table 1. For comparison, the redox potentials for the ZnPX

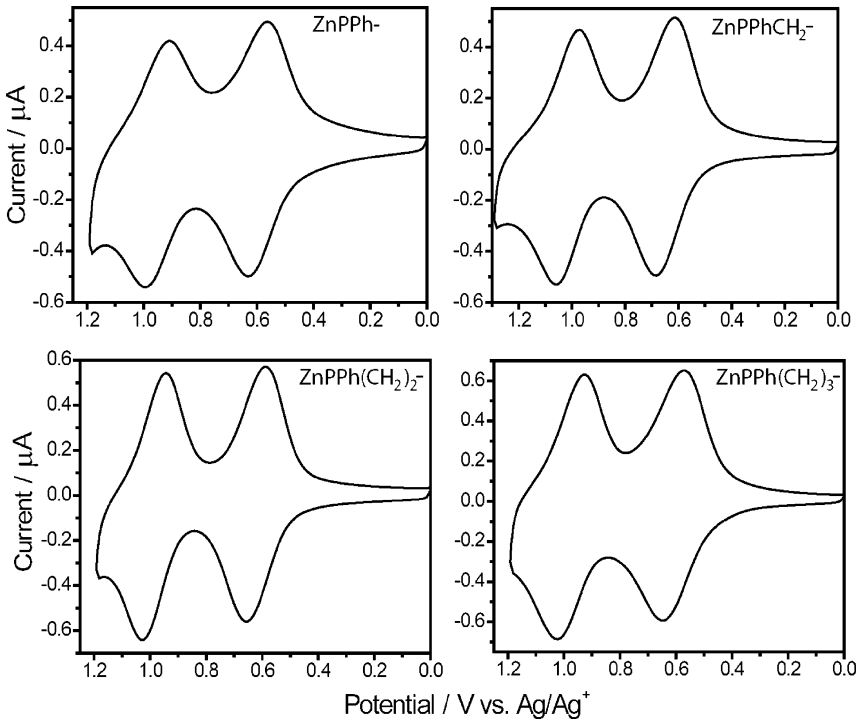

Figure 4. Representative fast-scan (100 V s^{-1}) voltammograms of the $ZnPPh(CH_2)_n-$ monolayers on Si(100).

and ZnPPhX porphyrins in solution are also included in Table 1. The salient observations from the voltammetric studies are summarized below.

(1) The redox potentials for the porphyrins in all of the monolayers are higher than those for the porphyrins in solution. This observation is consistent with our previous studies of other types of porphyrin monolayers, on both Si(100) and Au(111), which have shown that the redox potentials are influenced by both the packing density and screening from solvent and counterions.[2,3]

(2) The potentials for the $ZnPPh(CH_2)_n-$ class of monolayers are, on average, somewhat more shifted from their solution values than are those of the $ZnP(CH_2)_n-$ class of monolayers. Again, our previous work has indicated that more densely packed or heavily screened monolayers typically exhibit higher redox potentials.[2,3] In the systems reported here, the saturation surface coverage for the $ZnPPh(CH_2)_n-$ class of monolayers is, on average, higher than that for the $ZnP(CH_2)_n-$ class.

(3) The voltammetric waves of the $ZnPPh(CH_2)_n-$ class of monolayers are generally narrower than those of the $ZnP(CH_2)_n-$ class of monolayers, indicating that the thermodynamics of the redox process are more homogeneous for the former type of monolayers.

(4) The monolayers anchored to Si via C atoms are generally more stable than those anchored via O, S, or Se atoms, as evidenced by the voltammetric signatures observed after repeated cycling at 100 V s^{-1}.

2. Electron-Transfer Characteristics. Standard electron-transfer rate constants, k^0, were measured for the first oxidation process ($E^{0/+1}$) of the $ZnP(CH_2)_n-$ and $ZnPPh(CH_2)_n-$ monolayers at a variety of coverages in the low 10^{-12} to mid 10^{-11} mol cm^{-2} range. The interest in this surface-concentration dependence of the electron-transfer rates stems from our previous studies on porphyrin monolayers, on both Si(100) and Au(111), which show that the electron-transfer rates depend on surface coverage.[2d,g,3a,c] Unfortunately, owing to experimental limitations, the electron-transfer rates could not be measured at very high surface concentrations, i.e., those near saturation coverages. Nevertheless, the available concentration range is wide enough to detect significant variations in k^0.

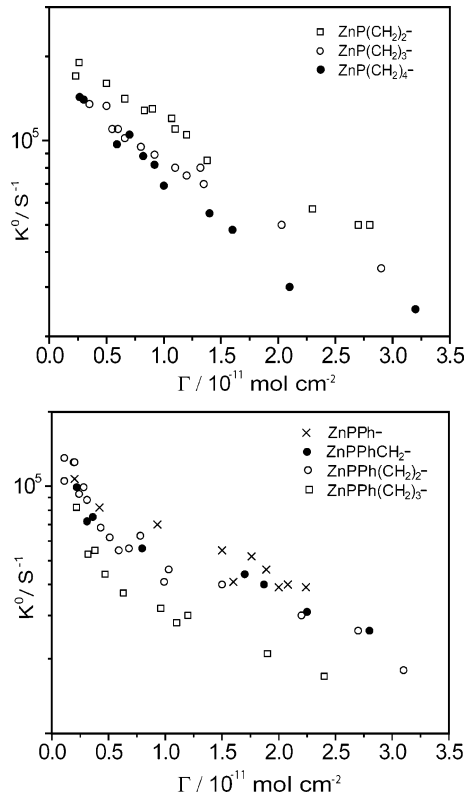

Figure 5. Standard electron-transfer rate constants, k^0, versus surface concentration, Γ, for the first oxidation process ($E^{0/+1}$) of the $ZnP(CH_2)_n-$ (top panel) and $ZnPPh(CH_2)_n-$ (bottom panel) monolayers on Si(100).

The electron-transfer rates as a function of surface concentration are shown in Figure 5 for each of the $ZnP(CH_2)_n-$ and $ZnPPh(CH_2)_n-$ monolayers. Inspection of the kinetic data for the porphyrin monolayers reveals the following trends.

(1) The electron-transfer rates for all of the monolayers decrease with increasing surface concentration, the same as in other types of porphyrin monolayers on both Au(111) and Si(100).[2d,g,3a,c]

(2) On average, the electron-transfer rates for the $ZnP(CH_2)_n-$ class of monolayers are faster than those of the $ZnPPh(CH_2)_n-$ class of monolayers. This is also consistent with our early studies on $ZnP(CH_2)X-$ and $ZnPPh(CH_2)X-$ (X = O, S, Se) monolayers on Si(100),[3c] for which the tethers are structurally similar to those of the $ZnP(CH_2)_2-$ and $ZnPPh(CH_2)_2-$ molecules examined in the present study. However, there is overlap in the rate regimes for the $ZnP(CH_2)_n-$ and $ZnPPh(CH_2)_n-$ classes of monolayers. In particular, the rates for the longer tethered members of the former class, $ZnP(CH_2)_3-$ and $ZnP(CH_2)_4-$, fall within the range of those of the shorter tethered members of the latter class, ZnPPh− and $ZnPPhCH_2-$.

(3) Within each class of $ZnP(CH_2)_n-$ and $ZnPPh(CH_2)_n-$ monolayers, the electron-transfer rates decrease as the number of methylene groups in the linker increases. This trend is less apparent at very low surface concentrations, even after accounting for the fact that the rates determined from the data at the lowest coverages are somewhat less certain owing to the very small currents involved.

(4) The rate versus surface-coverage plots for all of the $ZnP(CH_2)_n-$ monolayers are approximately log-linear, suggesting that a single type of process dictates the observed behavior. Approximate log-linear behavior is also seen for the shortest tethered member of the $ZnPPh(CH_2)_n-$ class of monolayers, i.e., ZnPPh−. As methylene spacers are added to the phenyl ring, however, the rate versus surface-coverage plots develop a curvature, which is most apparent for the longest tethered member of the $ZnPPh(CH_2)_n-$ class of monolayers, i.e., $ZnPPh(CH_2)_4-$. The curvature in the plots is indicative of the onset of another type of rate-controlling process as the surface coverage increases. We note that similar trends are observed in the rate versus surface coverage for the chalcogenide-tethered $ZnP(CH_2)X-$ and $ZnPPh(CH_2)X-$ (X = O, S, Se) monolayers on Si(100):[3c] the plots for the $ZnP(CH_2)X-$ monolayers exhibit log-linear behavior, whereas the plots for the $ZnPPh(CH_2)X-$ monolayers exhibit two distinct log-linear regimes.

3. Charge-Retention Characteristics. Charge-retention half-lives, $t_{1/2}$, were measured at selected surface coverages for the first oxidation state of the $ZnP(CH_2)_n-$ and $ZnPPh(CH_2)_n-$ monolayers, in parallel with the studies of the electron-transfer kinetics. Again, the interest in this surface-concentration dependence of charge retention stems from our previous studies on porphyrin monolayers, on both Si(100) and Au(111), which show that this process also depends on surface coverage.[2d,g,3a] As is the case for the measurement of the electron-transfer rates, experimental limitations preclude determination of the charge-retention times at the very highest surface concentrations. Nevertheless, the available concentration range is wide enough to detect significant variations in $t_{1/2}$.

The charge-retention half-lives as a function of surface concentration are shown for each of the $ZnP(CH_2)_n-$ and $ZnPPh(CH_2)_n-$ monolayers in Figure 6. The trends observed in the charge-retention times qualitatively parallel those observed for the electron-transfer rates.

(1) The charge-retention times for all of the monolayers increase (charge-dissipation rates decrease) as the surface concentration increases, consistent with previous observations on other types of porphyrin monolayers on both Au(111) and Si(100).[2d,g,3a]

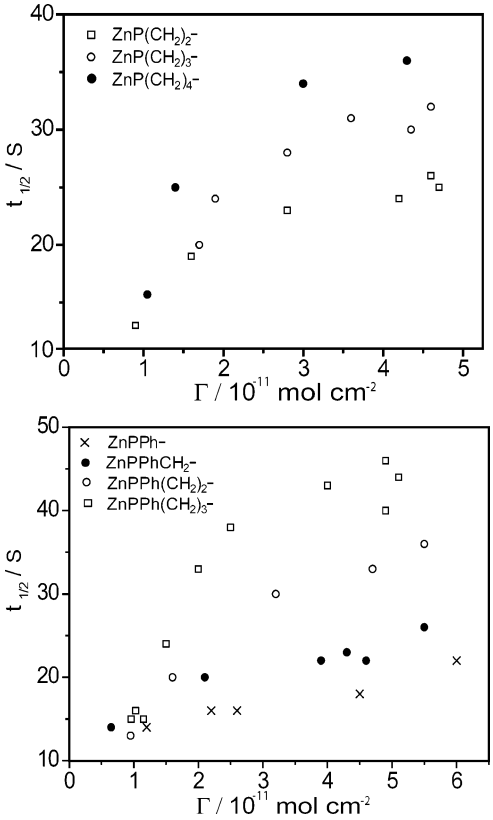

Figure 6. Charge-retention half-lives, $t_{1/2}$, versus surface concentration, Γ, for the first oxidation state of the $ZnP(CH_2)_n-$ (top panel) and $ZnPPh(CH_2)_n-$ (bottom panel) monolayers on Si(100).

(2) Differences in the charge-retention characteristics for the $ZnP(CH_2)_n-$ versus $ZnPPh(CH_2)_n-$ classes of monolayers are less distinct than those in their electron-transfer rates. In particular, the charge-retention curves for all three of the $ZnP(CH_2)_n-$ monolayers fall within those of the $ZnPPh(CH_2)_n-$ monolayers. The charge-retention times for all of the $ZnP(CH_2)_n-$ monolayers are longer than those of ZnPPh− but shorter than those of $ZnPPh(CH_2)_4-$.

(3) Within each class of $ZnP(CH_2)_n-$ and $ZnPPh(CH_2)_n-$ monolayers, the charge-retention times increase as the number of methylene groups in the linker increases. Also, as is the case for the electron-transfer rates, this trend is less apparent at very low surface concentrations. Again, the charge-retention times determined from the data at the lowest coverages are somewhat less certain owing to the very small currents that must be measured.

(4) The plots of charge-retention half-life versus surface coverage for all of the $ZnP(CH_2)_n-$ and $ZnPPh(CH_2)_n-$ monolayers exhibit significant curvature, with the exception of those for ZnPPh− and $ZnPPhCH_2-$. None of the plots are log-linear when plotted as the reciprocal of the half-life versus coverage, indicating multiple processes affecting the charge-retention characteristics. Similar behavior has been observed previously for $ZnPCH_2O-$ monolayers on Si(100).[3a]

IV. Discussion

The studies reported herein on the series of $ZnP(CH_2)_n-$ and $ZnPPh(CH_2)_n-$ classes of monolayers permit a systematic exploration of the factors that influence the adsorption geometry and packing density of those monolayers on the Si(100) surface, and how such structural characteristics influence the various charge-transfer processes that occur between the redox center

and the surface. We will address these issues in more detail below. We note at the outset that many of the general structural and charge-transfer characteristics exhibited by the $ZnP(CH_2)_n-$ and $ZnPPh(CH_2)_n-$ monolayers are similar to those we have previously reported for structurally related porphyrin monolayers on both Au(111) and Si(100).[2,3] Consequently, we will not discuss these features in detail. The reader is referred to our earlier publications for a more detailed discussion of these issues.

One very general conclusion that emerges from the present study is that attachment of porphyrin molecules to Si(100) via C-anchor atoms yields monolayers whose adsorption geometry, packing density, and charge-transfer characteristics are very similar to those of porphyrins bearing an identical linker but terminated with an O, a S, or a Se anchor atom. This observation adds to the body of data that indicates that the physicochemical characteristics of the monolayers are primarily controlled by the porphyrin molecule and appended linker rather than the anchor atom. Accordingly, molecular design strategies aimed at tuning properties of porphyrin (and likely other types of) monolayers must focus on the former rather than latter structural elements. The choice of anchor atom should be based mostly on issues related to the chemical stability of the monolayer.

A second observation derived from the present work is that porphyrins tethered to Si surfaces via very short alkyl linkers, i.e., $ZnP(CH_2)_n-$ ($n = 2-4$), all form monolayers with very similar adsorption geometries and packing densities (Table 1). In general, the short alkyl linkers yield monolayers that are less densely packed and in which the porphyrins are more tilted with respect to the surface normal than monolayers tethered with longer phenylalkyl tethers, i.e., $ZnPPh(CH_2)_2-$ and $ZnPPh(CH_2)_3-$. Interestingly, the ZnPPh− and $ZnPPhCH_2-$ monolayers, in which the porphyrins are linked to the surface through only a phenyl or benzyl group, exhibit adsorption geometries and packing densities that are qualitatively more similar to those of the $ZnP(CH_2)_n-$ monolayers than those of the monolayers bonded via the longer phenylalkyl tethers. These observations suggest that neither the short alkyl nor short aryl linkers possess sufficient torsional flexibility to optimize the packing of the porphyrin molecules on the surface. This constraint is overcome only when at least a second methylene group is added to the phenyl linker, at which point a more densely packed monolayer is obtained; packing is further enhanced when the third methylene group is added. The ability of the porphyrins with the longer phenylalkyl tethers to pack more densely appears to relate to their ability to stand more upright on the surface (Table 1), which ultimately must be due to the larger torsional flexibility of the longer phenylalkyl linkers. We also note that the fact that the average tilt angles for the ZnPPh− and $ZnPPhCH_2-$ monolayers are similar to those of the $ZnP(CH_2)_n-$ monolayers indicates that any steric interactions between the relatively bulky phenyl ring in the tether and the surface appear to be minimal and to not affect the molecular orientation.

A third theme that emerges from this work is that the charge-transfer characteristics for the molecules in a given class of C-anchored porphyrin monolayers as well as between the classes of monolayers follow trends that are qualitatively consistent with those expected on the basis of previous studies.[2d,3c] In particular, both the electron-transfer and charge-dissipation rates decrease (charge-retention times increase) as the length of the tether increases (Figures 5 and 6), qualitatively consistent with the expected dependence of electron transfer on distance. On the other hand, at all surface concentrations studied, the falloff in electron-transfer rate as the number of methylene units increases is less steep than predicted from the expression proposed for tunneling or through-bond mechanisms, $k^0 \propto \exp[-\beta d]$, where $\beta \approx 1.0$ per methylene unit.[15] This deviation from exponential behavior can be attributed to space−charge effects,[2d] because the simple exponential rate−distance dependence is only expected with redox centers that are electrically isolated from one another, and that condition is only met in extremely dilute monolayers with surface charge densities considerably lower than those for the monolayers investigated herein. It was also observed here that the addition of the phenyl ring to the linker further slows the electron-transfer rate: on average, the effect of the phenyl ring on the electron-transfer rates is equivalent to that of adding two or three methylene groups. It should be noted that steric constraints preclude coplanarity of the phenyl and porphyrin rings;[16] thus, significant π-conjugation between the two rings is not possible. The effect of the addition of the phenyl ring on the charge-retention times is not straightforward, as evidenced by the fact that the charge-retention times for the $ZnP(CH_2)_n-$ monolayers are nested among those of the $ZnPPh(CH_2)_n-$ monolayers. We have no explanation for this observation.

A fourth observation derived from the present work is that there appears to be a correlation between the trends observed in the plots of electron-transfer rate versus surface coverage and the ability of the porphyrin to assume a more upright orientation on the surface. In particular, the $ZnP(CH_2)_n-$ and the ZnPPh− monolayers all exhibit log-linear plots of rate versus surface coverage (Figure 5), strongly suggesting that this behavior is dominated by a single process. The plots begin to deviate from log-linear behavior in the case of the $ZnPPhCH_2-$ and/or $ZnPPh(CH_2)_2-$ monolayers, and distinctly depart from log-linear behavior in the case of the $ZnPPh(CH_2)_3-$ monolayers, a trend that parallels that observed for the average tilt angles of the monolayers (Table 1). In this connection, we have previously determined that the adsorption geometry can change with coverage, with the porphyrin ring tilting to a more upright orientation as the surface becomes more crowded.[2d] A change in adsorption geometry could introduce additional factors that mediate the electron-transfer rate as a function of surface coverage. We note, however, that the average tilt angles are measured for saturation coverage monolayers, whereas the deviation from log-linear behavior is observed at much lower surface concentrations. Plausibly, a change in adsorption geometry begins at a lower concentration regime with the longer tethers, hence the onset of additional processes controlling the rates. Unfortunately, it has not been possible to measure the average tilt angle in the low concentration regime (because the IR signals are too weak) to directly test this hypothesis. If a change in surface orientation does occur in the low concentration region, effects other than direct interactions between the porphyrins must play a role in determining charge transfer, because the average distance between the molecules at these surface coverages is quite large. Additional experiments with mixed monolayers are currently under way in our laboratory to further probe this transition.

V. Conclusions

The studies of the $ZnP(CH_2)_n-$ and $ZnPPh(CH_2)_n-$ classes of monolayers on Si(100) reported here provide new insights into the structural features that control packing density and adsorption geometry. These factors in turn underpin the thermodynamics and kinetics of electron transfer. The present studies indicate that both the structural and electron-transfer characteristics of the C-anchored porphyrin monolayers are similar to those of analogous monolayers anchored with O, S,

or Se atoms. The studies further indicate that optimal packing densities cannot be achieved for porphyrin monolayers with either short alkyl or short phenylalkyl tethers. Such densities can only be achieved when the tether has sufficient torsional flexibility to permit more upright orientations on the surface. The electron-transfer rates for both the $ZnP(CH_2)_n-$ and $ZnPPh(CH_2)_n-$ classes of monolayers monotonically decrease as the length of the linker increases. For both classes of monolayers, both the electron-transfer and charge-dissipation rates decrease monotonically as the surface coverage increases. Collectively, the studies reported provide clear evidence for the connection between adsorption geometry and charge-transfer behavior. A deep understanding of this relationship is essential for the informed design of molecular media for use as the active elements in information-storage applications.

Acknowledgment. This work was supported by the Center for Nanoscience Innovation for Defense and DARPA/DMEA (under Award Number H94003-04-2-0404) and by ZettaCore, Inc. We thank J. Diers for obtaining the solution electrochemical data.

References and Notes

(1) For reviews, see (a) Kwok, K. S.; Ellenbogen, J. C. *Mater. Today* **2002**, *5*, 28−37. (b) Carroll, R. L.; Gorman, C. B. *Angew. Chem., Int. Ed.* **2002**, *41*, 4378−4400.

(2) (a) Roth, K. M.; Dontha, N.; Dabke, R. B.; Gryko, D. T.; Clausen, C.; Lindsey, J. S.; Bocian, D. F.; Kuhr, W. G. *J. Vac. Sci. Technol., B* **2000**, *18*, 2359−2364. (b) Gryko, D.; Li, J.; Diers, J. R.; Roth, K. M.; Bocian, D. F.; Kuhr, W. G.; Lindsey, J. S. *J. Mater. Chem.* **2001**, *11*, 1162−1180. (c) Roth, K. M.; Lindsey, J. S.; Bocian, D.F.; Kuhr, W. G. *Langmuir* **2002**, *18*, 4030−4040. (d) Roth, K. M.; Gryko, D. T.; Clausen, C.; Li, J.; Lindsey, J. S.; Kuhr, W. G.; Bocian, D. F. *J. Phys. Chem. B* **2002**, *106*, 8639−8648. (e) Schweikart, K.-H.; Malinovskii, V. L.; Yasseri, A. A.; Li, J.; Lysenko, A.; Bocian, D. F.; Lindsey, J. S. *Inorg. Chem.* **2003**, *42*, 7431−7446. (f) Wei, L.; Padmaja, K.; Youngblood, W. J.; Lysenko, A. B.; Lindsey, J. S.; Bocian, D. F. *J. Org. Chem.* **2004**, *69*, 1461−1469. (g) Yasseri, A. A.; Syomin, D.; Malinovskii, V. L.; Loewe, R. S.; Lindsey, J. S.; Zaera, F.; Bocian, D. F. *J. Am. Chem. Soc.* **2004**, *126*, 11944−11953.

(3) (a) Roth, K. M.; Yasseri, A. A.; Liu, Z.; Dabke, R. B.; Malinovskii, V.; Schweikart, K.; Yu, L.; Tiznado, H.; Zaera, F.; Lindsey, J. S.; Kuhr, W. G.; Bocian, D. F. *J. Am. Chem. Soc.* **2003**, *125*, 505−517. (b) Liu, Z.; Yasseri, A. A.; Lindsey, J. S.; Bocian, D. F. *Science* **2003**, *302*, 1543−1545. (c) Yasseri, A. A.; Syomin, D.; Loewe, R. S.; Lindsey, J. S.; Zaera, F.; Bocian, D. F. *J. Am. Chem. Soc.* **2004**, *126*, 15603−15612.

(4) Liu, Z.; Yasseri, A. A.; Loewe, R. S.; Lysenko, A. B.; Malinovskii, V. L.; Zhao, Q.; Surthi, S.; Li, Q.; Misra, V.; Lindsey, J. S.; Bocian, D. F. *J. Org. Chem.* **2004**, *69*, 5568−5577.

(5) For reviews, see: (a) Song, J. H.; Sailor, M. J. *Comments Inorg. Chem.* **1999**, *21*, 69−84. (b) Buriak, J. M. *Chem. Commun.* **1999**, 1051−1060. (c) Hamers, R. J.; Coulter, S. K.; Ellison, M. D.; Hovis, J. S.; Padowitz, D. F.; Schwartz, M. P.; Greenlief, C. M.; Russell, J. N., Jr. *Acc. Chem. Res.* **2000**, *33*, 617−624. (d) Buriak, J. M. *Chem. Rev.* **2002**, *102*, 1271−1308. (e) Bent, S. F. *Surf. Sci.* **2002**, *500*, 879−903. (f) Stewart, M. P.; Buriak, J. M. *Comments Inorg. Chem.* **2002**, *23*, 179−203.

(6) Bateman, J. E.; Eagling, R. D.; Worrall, D. R.; Horrocks, B. R.; Houlton, A. *Angew. Chem., Int. Ed.* **1998**, *37*, 2683−2685.

(7) Li, X. Y.; Czernuszewicz, R. S.; Kincaid, J. R.; Su, Y. O.; Spiro, T. G. *J. Phys. Chem.* **1990**, *94*, 31−47.

(8) Li, X. Y.; Czernuszewicz, R. S.; Kincaid, J. R.; Spiro, T. G. *J. Am. Chem. Soc.* **1989**, *111*, 7012−7023.

(9) Silverstein, R. M.; Bassler, G. C. *Spectrophotometric Identification of Organic Compounds*; Wiley: New York, 1967.

(10) Painter P. C.; Coleman, M. M.; Koenig, J. L. *The Theory of Vibrational Spectroscopy and Its Application to Polymeric Materials*; Wiley: New York, 1982.

(11) Allara, D. L.; Nuzzo, R. G. *Langmuir* **1985**, *1*, 52−66.

(12) Harrick, N. J.; Mirabella, F. M. *International Reflection Spectroscopy: Review and Supplement*; Harrick Scientific Corp.: New York, 1985.

(13) Greenler, R. G. *J. Chem. Phys.* **1966**, *44*, 310−315.

(14) Zaera, F. *Int. Rev. Phys. Chem.* **2002**, *21*, 433−471.

(15) (a) Chidsey, C. E. D. *Science* **1991**, *251*, 919−922. (b) Smalley, J. F.; Feldberg, S. W.; Chidsey, C. E. D.; Linford, M. R.; Newton, M. D.; Liu, Y.-P. *J. Phys. Chem.* **1995**, *99*, 13141−13149.

(16) Scheidt, W. R.; Kastner, M. E.; Hatano, K. *Inorg. Chem.* **1978**, *17*, 706−710.